TEM characterization of metal and metal oxide particles supported by multi-wall carbon nanotubes

F. Liu · X. B. Zhang · D. Häussler · W. Jäger ·
G. F. Yi · J. P. Cheng · X. Y. Tao · Z. Q. Luo ·
S. M. Zhou

Abstract Composites of Sn–Pd particles and multi-walled carbon nanotubes (MWNTs), and of Ni–Co particles and MWNTs were investigated by transmission electron microscopy (TEM), energy-dispersive X-ray spectroscopy (EDS) and X-ray diffraction (XRD). The Sn–Pd particle composites were prepared by impregnation deposition, and the Ni–Co particle composites were prepared by electroless deposition on MWNTs synthesized by a chemical vapor deposition method using thermal catalytic decomposition of hydrocarbon. The morphologies and the microstructure of the deposited particles were investigated upon annealing the composites with and without hydrogen. Both the crystalline particle structure and the particle morphology are observed to be different for the samples annealed with and without hydrogen.

Introduction

Carbon nanotubes (CNTs) attract increasing attention due to their unique physical and chemical properties. Metal and metal-oxide particles supported by carbon nanotubes

F. Liu · X. B. Zhang · G. F. Yi · J. P. Cheng · X. Y. Tao ·
Z. Q. Luo · S. M. Zhou
State Key Laboratory of Silicon Materials, Department of
Materials Science and Engineering, Zhejiang University,
Hangzhou 310027, P.R. China

D. Häussler · W. Jäger (✉) · F. Liu
Microanalysis of Materials, Faculty of Engineering,
Christian-Albrechts-University (CAU) Kiel, Kaiserstrasse 2,
24143 Kiel, Germany EU
e-mail: wj@tf.uni-kiel.de

are expected to be potential future materials for hydrogenation catalysis or as materials for applications in Li-ion batteries, supercapacitors, magnetic recording, or for microwave absorption [1–7]. The chemical activity of composites of metal and metal-oxide particles with CNTs will depend not only on particle shape, size and chemical composition, but also on their distributions within the CNT materials. These parameters can be controlled by the specifications applied during their preparation and treatment.

Oxides, for example SnO_2, are the most frequently used materials for chemical gas sensors [8]. Pd and its oxides are important electrochemical and chemical catalysts used in many areas [2]. The use of noble metals, such as Pd or Pt, is expected to increase the catalytic sensitivity of SnO_2 [9]. Transition metals, such as Ni, Co and Fe, usually have magnetic properties, and many interesting particle phenomena and applications have been explored [10, 11].

The impregnation method is a widely used method for the preparation of sensing material particles and is characterized by its low cost, its high reproducibility and its potential to be used for mass production. It is reported that by this method Pd can be added to SnO_2 nanopowders using $SnCl_2$ as a reductor [9]. The process consists of several steps in which a metal salt is dissolved in an appropriate solution, the support material is mixed into the solution, and the mixture is subsequently dried by evaporating the solvent, thus finally obtaining a particle distribution on the support material.

The Ni or Co electroless deposition method has many favorable properties that allow large-scale applications [11–13]. Other applications are coatings of high thermal stability, diffusion barriers and contacts. Usually the wetability of the surfaces of the CNTs support materials for

the deposited coating or particles is poor. Here, the Sn (II) salt and Pd (II) salt solutions are well known agents that are able to sensitize and activate the initially inert surfaces for the further electroless deposition of other metals, such as Cu and Ni [14, 15].

The aim of this paper is to study the morphologies and the microscopic structure of particles and their spatial distributions on CNTs support for different technologically promising annealing treatments. Composites of Sn–Pd particles and MWNTs prepared by the impregnation method and composites of Ni–Co particles and MWNTs prepared by electroless deposition are investigated. TEM methods including EDS and XRD are used to characterize the particle morphologies and their microstructure as well as their spatial distributions.

Experimental procedures

In this section, the main steps of the preparation of the particle-MWNTs composite materials are briefly summarized. The MWNTs were synthesized by a chemical vapor deposition technique using a thermal catalytic decomposition of hydrocarbons [16, 17]. Two methods were used for the fabrication of nanoparticle-MWNT composites, which are described below.

Sn and Pd impregnation

The Sn and Pd impregnation on MWNTs were prepared in two steps: first, 1 g CNT powder was put into a 50 ml 0.044 M $SnCl_2$ aqueous solution and stirred magnetically for 30 min. Then the product was diluted with distilled water. Secondly, following filtering, the powder was mixed into a 50 ml 0.0023 M $PdCl_2$ solution for 24 h and subsequently washed, filtered again and dried.

Ni and Co electroless deposition

The as-prepared CNTs were stirred in 30 ml 0.5 M $SnCl_2$ aqueous solution (sensitization) and 30 ml 0.0023 M $PdCl_2$ solution (activation) respectively for 30 min, each step was followed by washing and filtering. Thereafter for metal deposition, the CNTs were put into a Ni bath and a Co bath, respectively. The composition of the bath solution and the deposition conditions are given in Table 1. The powder materials obtained were dried at 100 °C.

Annealing treatments

The annealing treatments of the powder material resulting from the impregnation and electroless deposition were performed in an open tube furnace at 700 °C for 30 min. During annealing the samples were exposed to a flow of pure H_2 (99.9% purity) or a flow of air, respectively. Subsequently, the samples annealed with hydrogen were cooled to room temperature in a nitrogen atmosphere. The samples annealed without hydrogen were cooled without any protecting gas atmosphere.

Characterization

Microscopic characterization was performed by transmission electron microscopy (TEM), using a Philips CM30 operated at 300 kV, and combined with spatially resolved microchemical analyses using EDS (spot diameter of approximately 17.5 nm). All EDS spectra shown in Figs. 2, 4, 7, 9 contain also spectral lines due to Cu and C because the sample materials have been mounted on Cu-grid supported C films. The results are compared with structure characterizations by XRD using Cu K_α radiation ($\lambda = 0.1541$ nm, Seifert XRD 3000) for a range of scattering angles 2θ from 20° to 80°.

Results

Sn–Pd impregnation—effects of annealing treatments

Figure 1 shows an example of the morphology of the Sn–Pd particle-CNT composite sample after annealing with hydrogen. The TEM bright-field micrograph reveals that the particles are dispersed on the MWNT bundles and adhere to the walls. Particles are observed in almost all CNT bundles, and their overall distribution is rather homogeneous, with only small fluctuations of the volume density within the composite. The particle sizes range from a few nanometers up to several tens of nanometers. A fraction of the particles clearly possess a core-shell structure (Fig. 1a, inset). Local EDS measurements taken on the core-shell structure particles (Fig. 2, Table 2)

Table 1 Composition of the bath solutions and deposition conditions used for the fabrication of Ni–Co–CNT composites by electroless deposition

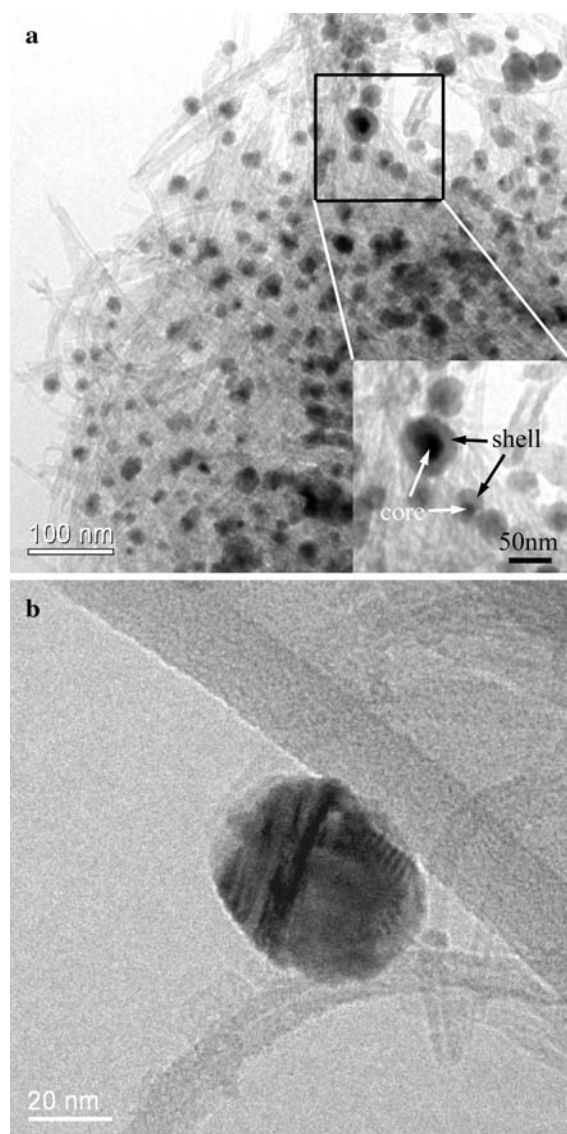| Ni bath composition	Concentration (g/l)	Co bath composition	Concentration (g/l)
$NiCl_2 \cdot 6H_2O$	20	$CoCl_2 \cdot 6H_2O$	30
$NaH_2PO_2 \cdot 2H_2O$	20	$NaH_2PO_2 \cdot 2H_2O$	20
$Na_3C_6H_5O_7 \cdot 2H_2O$	10	$Na_3C_6H_5O_7 \cdot 2H_2O$	35
NH_4Cl	35	NH_4Cl	50
Deposition condition			
pH value	9–10		
Temperature	85 °C		

Fig. 1 Sn–Pd impregnation: (**a**) distribution of Pd and Sn particles with core-shell (inset) structure dispersed uniformly on CNTs bundles after annealing with hydrogen, bright-field TEM micrograph. (**b**) A particle without core-shell structure, bright-field TEM micrograph. Contrast variations are ascribed to differently oriented crystalline parts of the particle. The weak contrast next to the particle is due to the C support film

Fig. 2 EDS measurements of Sn–Pd particle-CNT composites taken after annealing with hydrogen: (**a**), (**b**) spectra taken in the core and shell region, respectively, of a core-shell particle, displaying different relative fractions of Pd and Sn. (**c**) Spectrum taken from a particle without core-shell structure confirming the presence of Sn and O

indicate the presence of Pd and of Sn. These measurements reveal that the relative Pd signals are high for the projected core regions and largely absent for the shell regions, and that the relative Sn signals are high for the shell regions in most cases (Fig. 2a, b). Most of the particles without an obvious core-shell structure (Fig. 1b) consist of only Sn and O (Fig. 2c). Only a few of them possess in addition a small contribution of Pd.

Annealing without hydrogen results in the burning of the MWNT support material, leaving behind only the particles with sizes ranging between a few nanometers and hundreds
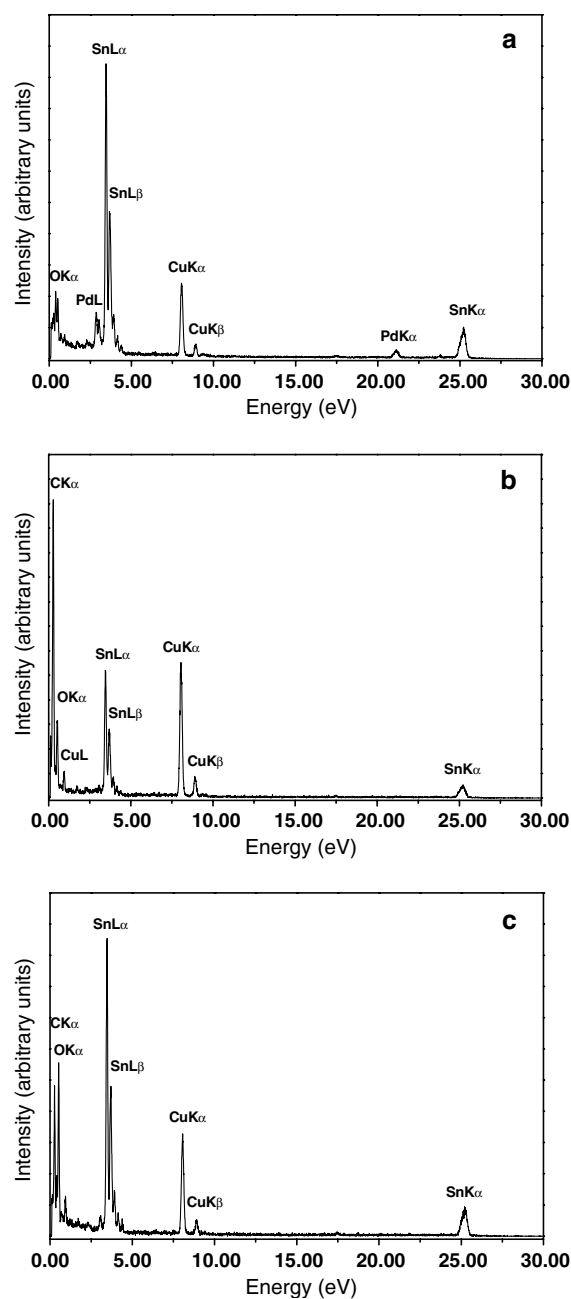
of nanometers. Figure 3 shows a TEM bright-field micrograph of a typical aggregate of such particles. Two types of particle morphology are observed: spherical-shaped particles with low contrast and polygon-shaped particles with high contrast. Spatially resolved EDS measurements (Fig. 4, Table 2) taken from individual particles indicate that the particles of predominantly spherical shape with

Table 2 Summary of particle compositions as obtained from spatially resolved EDS measurements for the Sn–Pd impregnation after two different annealing treatments

Element composition [wt%]	Annealing with hydrogen			Annealing without hydrogen	
	Core region of the core-shell particle	Shell region of the core-shell particle	Particle without core-shell structure	Spherical particle	Polygonal particle
Sn	88.9	90.0	92.1	61.3	0
Pd	9.1	1.6	0.3	0	91.9
O	2.0	8.4	7.6	38.7	8.1

low contrast show the presence of Sn and O signals (Fig. 4a). EDS spectra of polygon-shaped particles, which are characterized by strong contrast in TEM bright-field images, show the presence of Pd and O signals (Fig. 4b).

The XRD spectra measured after the annealing treatments are shown in Fig. 5. For the annealing with hydrogen the spectra display the presence of characteristic reflections, which agree well with previously reported peak positions for SnO_2 (JCPDS 41-1445), PdO (JCPDS 43-1024), Pd (JCPDS 46-1043), Sn (JCPDS 04-0673) and graphite (JCPDS 25-0284), respectively (Fig. 5a). The reflection of graphite is caused by CNTs. For the annealing without hydrogen the spectra show only SnO_2 and PdO reflections. No reflections due to diffraction from metal Sn, Pd or CNTs are detected (Fig. 5b). The presence of Pd and

Sn in particles has also been observed by the EDS measurements (Table 2). The major peaks can be attributed to the (110), (101) and (211) diffraction of crystalline SnO_2. The sharpness and intensity of these characteristic peaks are indicative of diffracting crystalline nanoparticles of rather high structural quality. In addition, few weak peaks are present in the spectra, which may result from remainders of catalyst material used for the growth of MWNTs.
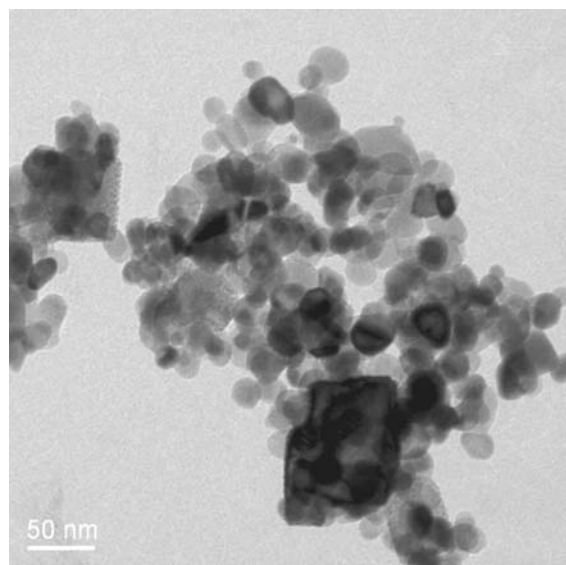

Fig. 3 Sn–Pd impregnation: distribution of polygon-shaped particles with high contrast and predominantly spherically shaped nanoparticles with low contrast after annealing without hydrogen. Particle sizes range from a few nanometers to hundreds of nanometers. The support of MWNTs has almost completely disappeared due to the treatment, bright-field TEM micrograph. Weak background contrast is caused by the C support film
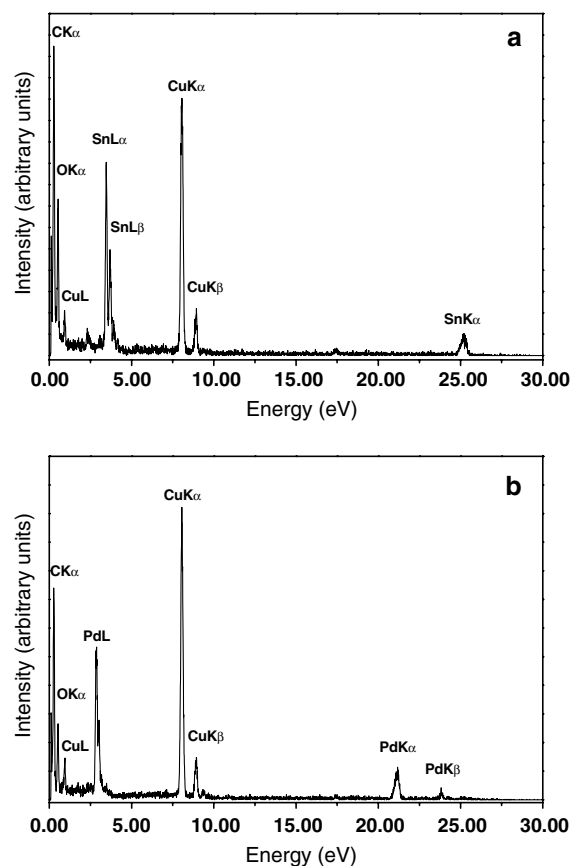

Fig. 4 EDS measurements of Sn–Pd particle-CNT composites taken after annealing without hydrogen: (**a**) spectrum taken from an area with particles of predominantly spherical shape, displaying a high relative fraction of Sn and O, (**b**) spectrum of a polygon-shaped particle, depicting the presence of a high relative fraction of Pd and O
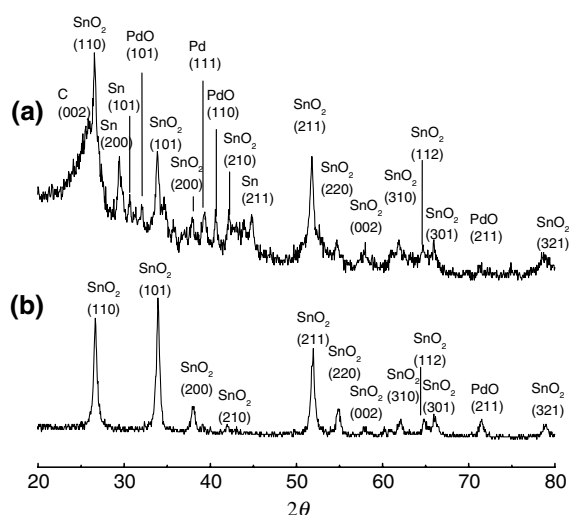
Fig. 5 Sn–Pd impregnation: XRD diagrams obtained after annealing (**a**) with and (**b**) without hydrogen. Indices of strongest intensity peaks are marked

Ni–Co electroless deposition—effects of annealing treatments

Figure 6a shows an example of the morphology of the Ni–Co particle-CNTs composite sample after annealing with hydrogen. The TEM bright-field micrograph shows that the Ni–Co particles are dispersed on the MWCNT bundles and adhere to the walls. The particle dimensions range from a few nanometers to hundreds of nanometers. A large fraction of these particles displays a core-shell structure. These particles possess a shell whose thickness is generally thinner compared to the case shown in Fig. 1a. The TEM bright-field image contrast of the core regions of some of the particles indicates that these particles consist of (at least) two different parts (Fig. 6b). Spatially resolved local EDS measurements reveal signals from Ni, Co, P, Sn and O (Fig. 7, Table 3). The core regions with high contrast are usually connected with relatively high Ni and P signals in the EDS spectra whereas core regions with low contrast are often connected with relatively high Co signals, indicating the presence of high fractions of the corresponding elements. The origin of the separation into two core regions is presently unclear and needs further investigation.

Figure 8 shows an example of a TEM bright-field image taken from the Ni–Co particle composite material after annealing without hydrogen. Some of the particles show a core-shell structure, however not as clearly displayed as for the sample annealed with hydrogen (Fig. 6a, b). Especially the core regions do not show the contrast differences as observed for the case shown by Fig. 6. The results obtained by spatially resolved local EDS measurements (Fig. 9, Table 3) reveal signals due to the presence of Ni, Co, Sn
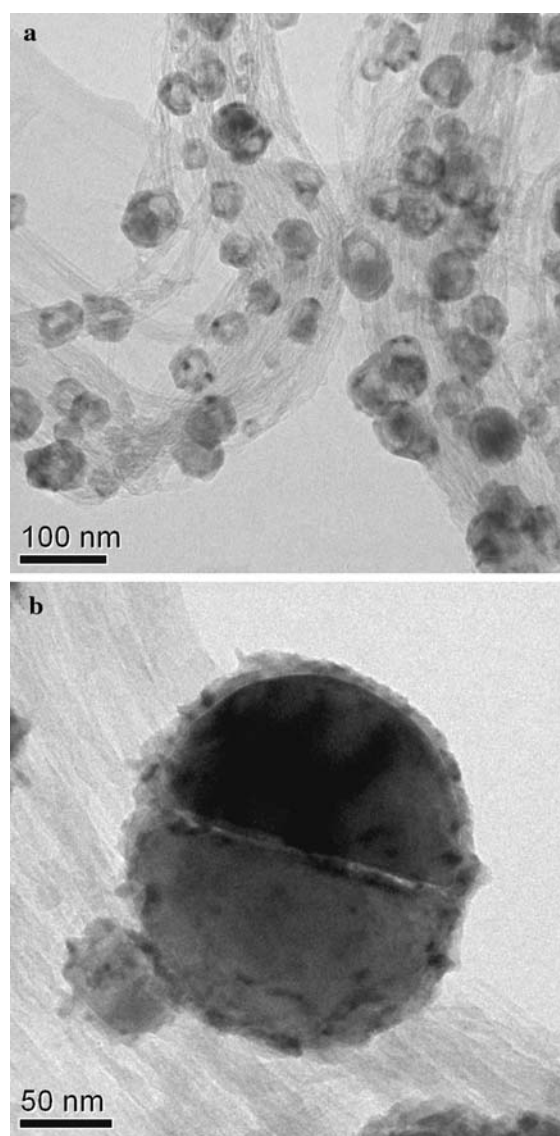

Fig. 6 Ni–Co electroless deposition: (**a**) particle-CNTs composite after annealing with hydrogen, bright-field TEM micrograph. Weak background contrast is caused by the C support film. (**b**) A larger particle showing a core-shell structure with regions of different contrast, bright-field TEM micrograph

and O. EDS results taken from core areas and from shell areas of particles generally show differences in the Co-to-Ni intensity ratios. In many cases the intensity of the Co signal is higher than that of the Ni signal (Fig. 9).

The XRD spectra of Ni–Co particle-CNT composites measured after the annealing treatments are shown in Fig. 10. For the annealing with hydrogen the spectra reveal sharp, high peaks due to the presence of crystalline Ni (JCPDS 04-0850). In addition peaks are detected that can be attributed to the presence of Ni$_3$P (JCPDS 34-0501), NiO (JCPDS 04-0835) and graphite (JCPDS 25-0284), respectively (Fig. 10a). The annealing treatment without
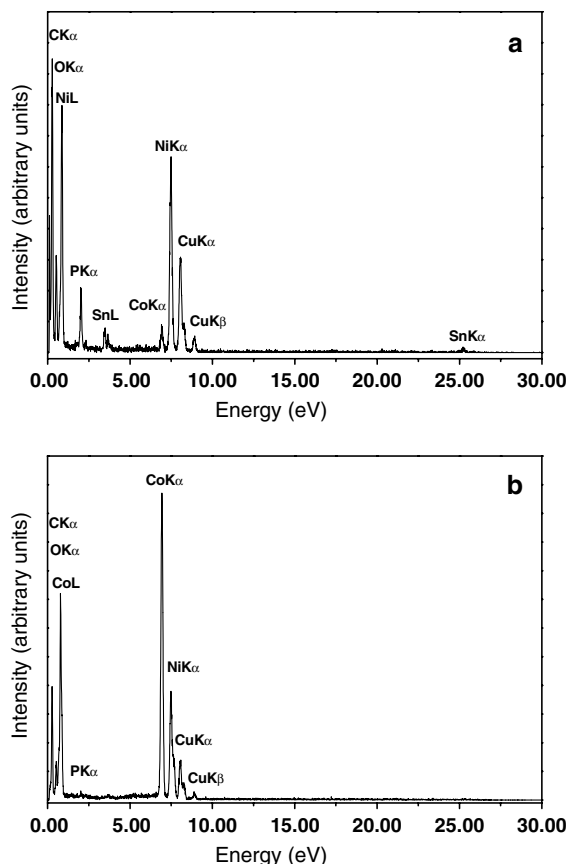
Fig. 7 EDS measurements of Ni–Co particle-CNTs composites taken after annealing with hydrogen: (**a**) spectrum taken from the core region with high contrast of a core-shell particle, displaying high relative Ni and P signals (**b**) spectrum taken from the core region with low contrast of a core-shell particle, depicting a high relative Co signal

hydrogen protection appears to result in a mainly non-crystalline particle structure. Some weak peaks are present which can be attributed to the reflections of crystalline Co_3O_4 (JCPDS 43-1003) (Fig. 10b).

Table 3 Summary of spatially resolved particle composition measurements by EDS for Ni–Co particle-CNT composites resulting from electroless deposition after annealing treatments

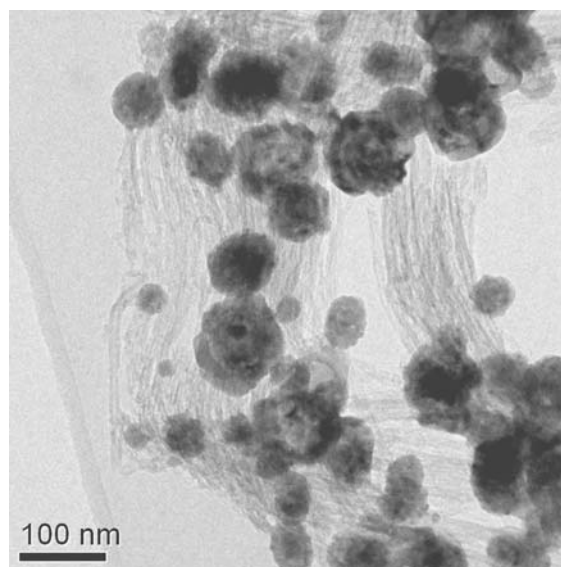| Element composition [wt%]	Annealing with hydrogen		Annealing without hydrogen
	High contrast region of a particle	Low contrast region of a particle	
Ni	56.7	22.3	17.2
Co	7.2	73.6	56.8
P	9.0	0.4	0.4
O	11.6	2.7	10.5
Sn	15.5	1.0	15.1

Fig. 8 Ni–Co electroless deposition: particle-CNTs composite after annealing without hydrogen, bright-field TEM micrograph. Weak background contrast is due to C support film

Discussion

In fabricating the Sn–Pd composites investigated in this study, in the first step, called impregnation, the CNTs support materials are immersed into aqueous precursor solutions of $SnCl_2$ and $PdCl_2$. After a period of stirring, the precursors will deposit and adhere to the surfaces of the CNT support materials. Subsequent treatments consist of washing and filtering (section Experimental procedures). Finally, particle-CNT composites are obtained which are exposed to the annealing treatments at high temperatures.

The fabrication of Ni–Co composites on CNT support materials used the electroless deposition method. In order to sensitize and chemically activate the surfaces of the
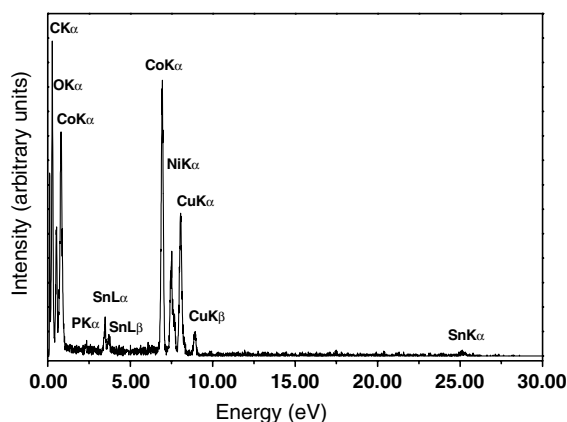

Fig. 9 EDS measurements of Ni–Co particle-CNT composites taken after annealing without hydrogen: spectrum taken from a particle region, displaying the presence of Ni, Co, Sn and O
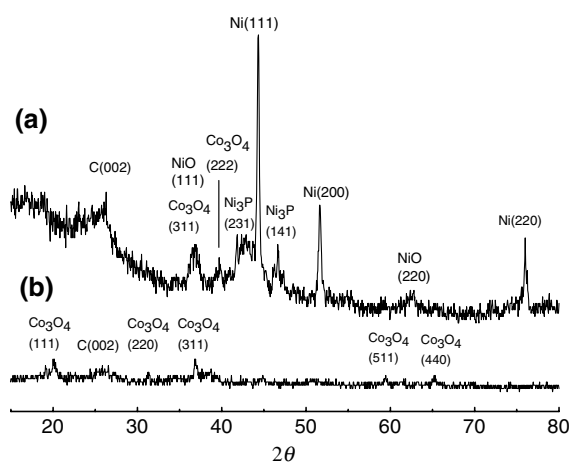
Fig. 10 Ni–Co electroless deposition: XRD diagram taken after annealing (**a**) with and (**b**) without hydrogen. Indices of strongest lines are marked

CNT materials, the same treatment as before has been applied, i.e. the CNT support materials are first immersed into aqueous precursor solutions of $SnCl_2$ and $PdCl_2$. This step is necessary since the surfaces of as-prepared CNTs are non-polar, and their wetability for metals, such as Ni or Co, is generally poor. In a following step, the treated CNT materials are put into a bath consisting of Ni or Co salts and a reducing agent. The Ni and Co salts will reduce to elemental Ni and Co, which will be deposited and assembled on the CNT material forming the composites.

For both the impregnation and electroless deposition, the particles of the composites are usually amorphous before annealing [13, 18]. As we have observed in our study (section Results) and will be discussed in more detail below, the annealing treatments investigated result in the formation of crystalline particles for the case of Sn–Pd composites, and, depending on the annealing treatment, in crystalline or non-crystalline particles for the case of Ni–Co composites. Oxidation of the particle materials may occur when the annealing is performed without a protecting atmosphere. Annealing the particle-support composites with hydrogen will prevent oxidization during annealing because of the presence of the reducing hydrogen.

Sn–Pd impregnation

During the first step of the Sn–Pd impregnation, the $SnCl_2$ is deposited on the wall surfaces of the CNTs. During the second step applied after rinsing the material in distilled water, $PdCl_2$ is deposited. The $PdCl_2$ will be reduced by $SnCl_2$ according to the reaction: $Pd^{2+} + Sn^{2+} \rightarrow Sn^{4+} + Pd$. The resulting products of this reaction are Pd and SnO_2. Some of the Pd may be oxidized because the impregnation is processing in the solution. The residual $SnCl_2$ can become $Sn(OH)_2$ after rinsing the composites in water. Residual

$SnCl_2$ or $Sn(OH)_2$ and $PdCl_2$ may cover the Pd or PdO as a sheath [14].

Sn–Pd impregnation—annealing with hydrogen

The annealing treatment with hydrogen at high temperature reduces some of the SnO_2 to elemental Sn [18]. Elemental Sn has a low melting temperature of nominally 232 °C. From the EDS results (Fig. 2a, b, Table 2), we speculate that Sn melts during the annealing at a temperature of 700 °C and covers the Pd or PdO resulting in core-shell structure particles which are distributed between the bundles of CNTs (Fig. 1a). The presence of high peak intensity in the XRD measurements (Fig. 5a), which is ascribed to crystalline SnO_2, indicates that the hydrogen annealing treatment has not reduced completely the SnO_2 present in the composites. This SnO_2 may result from the decomposition of $Sn(OH)_2$ at high temperature, a process which apparently leads to formation of the particles without a core-shell structure (Fig. 1b). The weak Pd signals in the EDS spectra of the particles without a core-shell structure (Fig. 2c, Table 2) indicate the possibility that Pd or PdO from residual $PdCl_2$ may become attached to the surface of the SnO_2 particles [9].

Sn–Pd impregnation—annealing without hydrogen

Annealing without hydrogen caused oxidation of the CNTs so that the CNTs disappeared by burning at the temperatures applied. Without the protecting gas, this burning of CNTs occurs at temperatures of 500–700 °C [19–22]. The Pd oxidizes and forms PdO particles, and oxidation of Sn particles presumably forms SnO_2 particles. The result is the formation of particle agglomerates without CNT support (Fig. 3). Presumably both the mechanical interlocking action of the CNT network and the inert surface largely hinder the coalescence of Sn, even in the molten state. It is reported that the CNTs can not only affect the nucleation during the oxide crystallization process but also prevent the coagulation and flocculation processes [19]. Although the tin oxidation temperature is above 550 °C [23], which is almost the same temperature the CNTs begin to burn, most of the particle sizes remain within the range of a few nanometers to several hundred nanometers. Both the PdO and the SnO_2 have a high melting temperature (870 °C and 1630 °C, respectively) so most of the particles will largely maintain their particle size during oxidation.

Ni–Co electroless deposition

After sensitization and activation of the CNTs, the catalyst for the further metal deposition, Pd, will reside on the CNT surfaces covered by layers of $Sn(OH)_2$. We name this

intermediate product as ''catalytic CNTs'' for further metal deposition. When the catalytic CNTs are immersed in the Ni deposition bath, the Sn(OH)$_2$ sheaths will be dissolved from the surfaces, creating surfaces of Pd catalyst on CNTs [14]. Then Ni ions will be reduced to Ni by the reducing agent in the Ni deposition bath solution at the proper temperature and pH value. The reduced Ni will preferentially be deposited at the Pd catalyst on the CNT surfaces and nucleate Ni particles by assembling more and more atoms at such sites. This process is named self-catalysis. Following the Ni deposition, the Co deposition is performed in the Co bath. At first, the Co will be deposited onto the existing Ni particles due to the self-catalysis effect. During both deposition steps also P present in the bath solution will be co-deposited with Ni and Co.

Ni–Co electroless deposition—annealing with hydrogen

It has been reported that the structure of the as-deposited electroless Ni–P is different for different phosphorus contents [24–26]. For P contents larger than 9 wt%, the deposits are amorphous upon deposition [24]. After heat treatment, the final phases of the deposit consist of stable crystalline Ni$_3$P and face-centered cubic (fcc) Ni [24, 25]. Following electrochemical deposition of Co–P, the structure of the deposit is amorphous when the P content is above 12 wt% [27]. At lower P concentrations the deposit consists of hexagonal-close-packed (hcp) Co nanocrystallites [28]. Annealing treatments may turn amorphous Co–P into a mixture of fcc Co and crystalline Co$_2$P [27].

Our experiments show that the electroless deposition method leads to the co-deposition of Ni and Co on the CNT materials. The results of the EDS measurements indicate that the P content of different particles is below 10 wt% (Table 3). During annealing with hydrogen at a temperature of 700 °C, particles with a core-shell structure depicting different contrast in the core area are formed (Fig. 6a, b). The XRD investigations of these composites show the presence of a mixture of Ni, Ni$_3$P, NiO, and Co$_3$O$_4$ (Fig. 10a). No Co$_2$P could be detected as has been reported in the literature [27]. Our EDS results confirm the presence of Co (Fig. 7, Table 3), which at room temperature has a crystalline hcp structure and will transform into an fcc structure during annealing at 600 °C [27]. However, both the diffraction reflections of hcp Co and of fcc Co, are overlapping with those of Ni and Ni$_3$P in XRD diagrams. Therefore, we could not distinguish the two possible Co structures from our measurements taken at common X-ray scan speeds. Considering the formation by the annealing treatment with hydrogen, the XRD results (Fig. 10a) and the EDS results (Fig. 7, Table 3) we speculate that the particles consist of metallic Ni (fcc), Co (fcc or hcp), Ni$_3$P, NiO and Co$_3$O$_4$. In agreement with spatially resolved EDS

measurements (Fig. 7, Table 3) locally different fractions of the various particle constituents occur, also explaining the contrast differences observed in bright-field TEM images (Fig. 6). Formation of oxides on the particles may not be excluded when the composites are exposed to air following the heat treatment.

SnCl$_2$ was used in the sensitization step before the electroless deposition of these composite materials. The presence of Sn signals connected with the particles is shown by the EDS spectra (Fig. 7, Table 3), however, the spatial distribution of Sn could not yet be determined. During the annealing treatment of the composites with hydrogen, the residual SnCl$_2$ may be reduced to elemental Sn, which, at the high temperature of about 700 °C, could melt. Our XRD measurements (Fig. 10a) indicate that the Sn is not present as crystalline elemental Sn, however.

Ni–Co electroless deposition—annealing without hydrogen

For annealing without a hydrogen atmosphere many of the observed particles possess also a core-shell structure, but do not show different contrast in the core region (Fig. 8). In the XRD measurements the presence of crystalline Co$_3$O$_4$ is detected (Fig. 10b). The rather low peak intensities indicate that the crystalline Co$_3$O$_4$ exists after annealing only in small amounts in these composites (Fig. 10b). This result, the absence of crystalline Ni in XRD (Fig. 10) and the fact that both Co and Ni are clearly seen by the EDS measurements (Fig. 9) suggest that most of the particles contain these materials in an amorphous phase or as nanometer-sized crystalline particles. This result is in agreement with reports describing that electroless Ni–P coatings on Cu sheets maintain their amorphous structure also during a heat treatment at 230 °C for 24 h [15]. Our spatially resolved EDS results of measurements taken from various particles showed variations of the local compositions within different particle areas, showing a tendency of a higher Co signal as compared to the Ni signal for many particles (Fig. 9, Table 3). In the preparation of the composites the Co deposition follows the Ni deposition. Therefore Co will preferentially reside on Ni-containing particles. Since the bath solution contains also P (Table 1) and since the EDS measurement of particles show the presence of P (Fig. 9) we conclude that the particles may consist of an amorphous Ni–P compound as has also been described in the literature [13, 15] or as a Ni–P–Co compound. We assume that during the annealing treatment without hydrogen some of the Co oxidizes thus forming Co$_3$O$_4$. Furthermore, most of the Co and Ni co-deposited with P will not be reduced to metallic Co and Ni and thus maintain an amorphous structure or reside as nanometer-sized crystalline cluster. However, further investigations

are necessary to confirm this assumption. The CNT support materials are stable during annealing without hydrogen, in contrast to the case of Pd–Sn composites (Fig. 3). The reason for this difference could be that the CNTs are covered by some chemical agents, such as Na_3-$C_6H_5O_7 \cdot 2H_2O$, remaining on their surfaces from the electroless deposition baths. Such agents would keep them from burning at the annealing temperature.

Summary and conclusions

Using the rather simple methods of impregnation and electroless deposition for the fabrication of particle-CNT composites, Sn, Pd, Ni and Co and presumably also their oxides could be distributed as particles rather uniformly on CNT support materials. The particle sizes ranged from a few nanometers up to several tens of nanometers.

The influences of different types of annealing treatments were investigated, and the following changes of the resulting morphologies were found:

– For the Sn–Pd particles obtained by the impregnation method, both particles with a core-shell structure, consisting of a Sn shell and a Pd or PdO core, and SnO_2 particles without an obvious core-shell structure, were observed following the hydrogen annealing treatments. After annealing treatments in air, polygonal PdO particles and spherical SnO_2 particles were observed.

– Ni–Co particles obtained from electroless deposition were found to possess a core-shell structure after annealing. Following hydrogen annealing, the deposited particles consist of two parts, namely crystalline Ni, NiO and Ni_3P phases and crystalline Co and Co_3O_4 phases. Annealing without hydrogen results in amorphous or nanometer-sized crystalline particles.

In conclusion, the annealing treatments with hydrogen for both Sn–Pd impregnation composites and Ni–Co electroless deposition composites, result in a reduction and crystallization of the initially deposited metals (Sn, Pd, Ni and Co). Characteristic of these metal particle-CNTs composites are the rather narrow particle size distributions and the uniform coverage of the CNT materials indicating that the CNT network prevents the formation of larger particles. Annealing without protecting atmosphere may induce oxidization of the metal particles, resulting in composites containing metal oxide particles (Sn–Pd) or amorphous or nanocrystalline particles (Ni–Co). For the Sn–Pd composites the annealing without hydrogen leads to formation of particle agglomerates without CNT support, representing a processing method, which allows preparing nanoparticles for catalysis without any support materials. Our results show that the morphology and structure of the Sn, Pd, Ni, Co particles and their corresponding oxide particles obviously can be influenced in different ways by the different annealing treatments.

References

1. Fullam S, Cottell D, Rensmo H, Fitzmaurice D (2000) Adv Mater 12:1430
2. Guo D, LI H (2005) J Colloid Interface Sci 286:274
3. Yoshitake T, Shimakawa Y, Kuroshima S, Kimura H, Ichihashi T, Kubo Y, Kasuya D, Takahashi K, Kokai F, Yudasaka M, Iijima S (2002) Physica B 323:124
4. Wu H, Cao Y, Yuan P, Xu H, Wei X (2005) Chem Phys Lett 406:148
5. Xu S, Li F, Wei R (2005) Carbon 43:855
6. Li Y, Ding J, Chen J, Xu C, Wei B, Liang J, Wu D (2002) Mater Res Bull 37:313
7. Xing Y (2004) J Phys Chem B 108:19255
8. Cheng B, Russell J, Shi W, Zhang L, Samulski E (2004) J Am Chem Soc 126:5972
9. Diaz R, Arbiol J, Cirera A, Sanz F, Peiro F, Cornet A, Morante J (2001) Chem Mater 13:4362
10. Zhang X, Wen G, Huang S, Dai L, Gao R, Wang Z (2001) J Magn Magn Mater 231:L9
11. Li D, Liu C, Conway P (2005) Circuit World 31:32
12. Chen T, Pogowski D, White R (1978) J Appl Phys 49:1816
13. Balaraju J, Rajam K (2005) Surf Coat Tech 195:154
14. Shukla S, Seal S, Akesson J, Oder R, Carter R, Rahman Z (2001) Appl Surf Sci 181:35
15. Gao J, Wu Y, Liu L, Hu W, (2005) Mater Lett 59:391
16. Li Y, Zhang X, Tao X, Xu J, Chen F, Huang W, Liu F (2004) Chem Phys Lett 386:105
17. Li Y, Zhang X, Tao X, Xu J, Huang W, Luo J, Luo Z, Li T, Liu F, Bao Y, Geise H (2005) Carbon 43:295
18. Wang Y, Lee J, Chen B (2004) J Electrochem Soc 151:A563
19. Xie J, Varadan V (2005) Mater Chem Phys 91:274
20. Cheng J, Zhang X, Ye Y, Tu J, Liu F, Tao X, Geise H, Van Tendeloo G (2005) Micropor Mesopor Mater 81:73
21. Cheng J, Zhang X, Liu F, Tu J, Ye Y, Ji Y, Chen C (2003) Carbon 41:1965
22. Kitiyanan B, Alvarez W, Harwell J, Resasco D (2000) Chem Phys Lett 317:497
23. Kolmakov A, Zhang Y, Moskovits M (2003) Nano Lett 3:1125
24. Guo Z, Keong K, Sha W (2003) J Alloy Compd 358:112
25. Keong K, Sha W, Malinov S (2002) J Alloy Compd 334:192
26. Keong K, Sha W, Malinov S (2002) J Mater Sci 37:4445
27. Kohn A, Eizenberg M (2003) J Appl Phys 94:3810
28. Admon U, Bar-Or A (1973) J Appl Phys 44:2300